Nickel enhanced graphene growth directly on dielectric substrates by molecular beam epitaxy

Joseph M. Wofford,[1,a)] Florian Speck,[2] Thomas Seyller,[2] Joao Marcelo J. Lopes,[1,a)] and Henning Riechert[1]
[1]*Paul-Drude-Institut für Festkörperelektronik, Hausvogteiplatz 5-7, 10117 Berlin, Germany*
[2]*Technische Universität Chemnitz, Institut für Physik, Reichenhainer Str. 70, 09126 Chemnitz, Germany*

(Received 19 January 2016; accepted 3 July 2016; published online 29 July 2016)

The efficacy of Ni as a surfactant to improve the crystalline quality of graphene grown directly on dielectric $Al_2O_3(0001)$ substrates by molecular beam epitaxy is examined. Simultaneously exposing the substrate to a Ni flux throughout C deposition at 950 °C led to improved charge carrier mobility and a Raman spectrum indicating less structural disorder in the resulting nanocrystalline graphene film. X-ray photoelectron spectroscopy confirmed that no residual Ni could be detected in the film and showed a decrease in the intensity of the defect-related component of the C1s level. Similar improvements were not observed when a lower substrate temperature (850 °C) was used. A close examination of the Raman spectra suggests that Ni reduces the concentration of lattice vacancies in the film, possibly by catalytically assisting adatom incorporation. *Published by AIP Publishing*. [http://dx.doi.org/10.1063/1.4958862]

I. INTRODUCTION

The potential of graphene as a transformative technological material has been well documented.[1] The practical realization of this potential has, however, continued to be hindered by the lack of a synthesis method which allows high-quality graphene to be grown directly on a technologically compatible dielectric substrate. A variety of different dielectric templates have been investigated in this context, including Al_2O_3,[2] SiC,[3] mica,[4] and Ge.[5] Addressing this synthesis shortcoming remains a central challenge in graphene research.

The microstructure of most graphene grown on dielectric substrates—often described as "nanocrystalline"—is composed of a multitude of small, sp^2-bonded domains with limited long-range order.[6,7] Estimates of the lateral dimension of these domains have ranged from 2 nm (Raman spectroscopy) to 180 nm (low-energy electron diffraction).[8,9] This microstructure is indicative of a static growth surface where C adatoms diffuse only minimally prior to their incorporation into a sp^2-bonded cluster, limiting the resulting domain size. The inability of C adatoms to diffuse to a preferential attachment site at the graphene growth front may further decrease the crystalline quality of the film through the introduction of point defects such as lattice vacancies. This structural disorder leads to a corresponding degradation of the film's electrical properties, dramatically reducing the utility of graphene grown directly on dielectric substrates.

A well-established method for manipulating growth kinetics to enhance film quality during vapor phase epitaxy of traditional thin-film semiconductors is the use of surfactants, or "surface-active species." Surfactants are often employed to promote planar, layer-by-layer growth during heteroepitaxy (i.e., Frank-van der Merwe as opposed to Stranski-Krastanov or Volmer-Weber growth); which they do by altering the relative surface free energies of the dissimilar film and substrate materials.[10] However, a surfactant can also function catalytically to alter the atomistic kinetics of crystal growth. The presence of a given concentration of immiscible species may substantially enhance the quality of crystal growth in some circumstances. An example of this is Pb in Si homoepitaxy. By altering the sequence of states occupied by a Si atom as it moves from the vapor phase towards incorporation into the Si lattice at a step kink, a minimal surface concentration of Pb can lower the substrate temperature required for high-quality crystal growth by 350 °C.[11] The development of an analogous technique in graphene growth would be advantageous in addressing the structural deficiency of graphene grown on dielectric substrates.

In this paper, we investigate the efficacy of Ni as a surfactant during graphene growth on $Al_2O_3(0001)$ by molecular beam epitaxy (MBE). Ni was chosen because its moderate chemical affinity with C makes it more likely to influence the graphene growth process than a less reactive metal such as Cu. For instance, the high-quality graphene films grown on Ni facets are tightly bound to the substrate,[12] and C is highly soluble in the bulk of the metal.[13] Despite this, graphene is regularly grown on Ni substrates without significant metal being incorporated into the lattice.[14] Ni also has a sufficiently high vapor pressure over the substrate temperature range accessible by MBE to make the complete re-evaporation of the metal feasible at the conclusion of C deposition.[15]

II. EXPERIMENTAL

Monolayer thick nanocrystalline graphene films, possibly with some slight localized thickness variations, were deposited on $Al_2O_3(0001)$ substrates via MBE (base pressure

a)Authors to whom correspondence should be addressed. Electronic addresses: joewofford@gmail.com, Tel.: +49.30.20377.426 and lopes@pdi-berlin.de, Tel.: +49.30.20377.327.

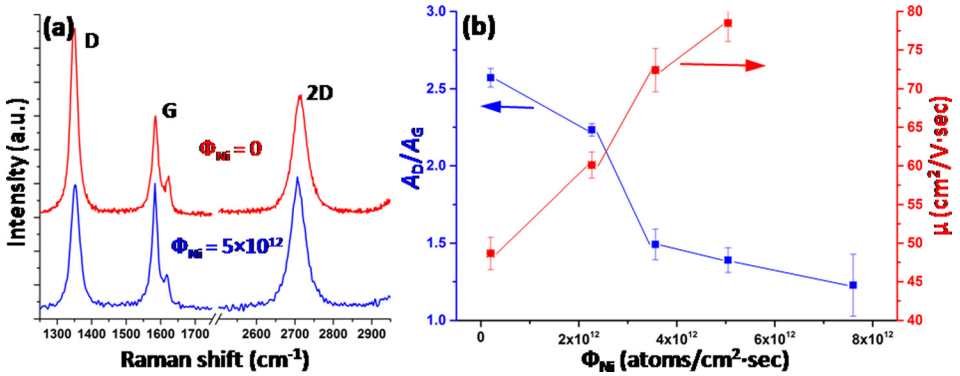

FIG. 1. Raman spectra from graphene grown with and without an applied Ni flux at a substrate temperature of 950 °C (a), showing the resulting decrease in D peak intensity (Φ_{Ni} is in atoms/cm^2·s). (b) The ratio of the integrated intensities of the Raman D and G peaks (A_D/A_G) and the charge carrier mobility (μ) as a function of applied Ni flux for graphene films grown at 950 °C. The mobility increases and A_D/A_G steadily decreases with increasing Ni flux, indicating decreasing crystalline disorder in the film ($\lambda = 473$ nm).

$\sim 2.5 \times 10^{-10}$ Torr). The 1 cm × 1 cm substrates were back-coated with 1 μm of Ti, cleaned with standard solvents, and outgassed at 300 °C for 60 min prior to deposition. Ni fluxes ranging from 2×10^{12} to 8×10^{12} atoms/cm^2·s were generated using a standard high-temperature effusion cell, evaporating 99.999% pure metallic Ni. If the entire Ni dose were retained on the substrate surface over each 244 min growth, these fluxes would correspond to uniform Ni films ~3 nm to ~12 nm thick. One of two different sources of elemental C was employed for each growth: a resistively heated pyrolytic graphite filament (MBE Komponenten GmbH, SUKO-type) or an electron-beam evaporator fitted with a pyrolytic graphite target (MBE Komponenten GmbH, EBVV63–4-S). Once calibrated to produce a flux of 3×10^{12} atoms/cm^2·s (corresponding to 20 min per graphene monolayer for a fully retained dose), the two C sources yielded equivalent results. Growths were performed at a substrate temperature of either 850 °C or 950 °C. The substrates were initially exposed to only the Ni flux for 4 min to allow the metal to accumulate on the surface prior to the start of C deposition (corresponding to a total dose of $\sim\frac{1}{4}$ to ~1 monolayer of Ni, although the actual resulting surface concentration was likely much lower). C was then deposited for 240 min while the Ni flux was maintained.

The resulting graphene films were characterized using a number of different methods, including atomic force microscopy (AFM) to examine their surface morphology. Micro-Raman spectroscopy measurements with a 100× objective offered information on the structural quality of the films. The Raman system used was a LabRAM HR Evolution from Horiba Scientific, with a 473 nm wavelength (λ) solid-state laser. X-ray photoelectron spectroscopy (XPS) was used to determine the elemental composition and binding state of the films, as well as the quantity of carbon deposited. The average thickness of the films was determined from the absolute intensity of the C1s level relative to a known monolayer graphene reference and confirmed via the C1s/Alp and C1s/O1s intensity ratios (both of which were consistent with the growth rate expected from previous experiments and the well-calibrated C sources). Measurements were performed under ultra-high vacuum conditions with a hemispherical analyzer (SPECS Phoibos 150). Al K_α radiation was provided by an X-ray source (SPECS XR 50 M) in combination with a monochromator (SPECS Focus 500). The samples were annealed up to 400 °C in vacuum prior to spectrum collection to remove surface contaminants. Finally, the Hall effect transport measurements yielded the charge carrier mobility and concentration within the graphene films. The transport measurements were performed in the van der Pauw configuration at room temperature with pressed metallic In contacts and a 0.3 T magnetic field.

III. RESULTS

The influence of a Ni flux on the properties of the graphene films was first examined by Raman spectroscopy, which is a valuable technique to assess the degree of crystalline perfection in graphene. Spectra representative of graphene grown with and without a Ni flux are shown in Figure 1(a), and both display the D (~1350 cm^{-1}), G (~1580 cm^{-1}), D′ (~1620 cm^{-1}), and 2D (~2700 cm^{-1}) peaks which are the signature of defective sp^2-bonded C, consistent with the nanocrystalline microstructure of the films. The D peak results from structural disorder in the graphene lattice[16]—such as small crystalline domain size or point defects—and its integrated intensity relative to the non-defect related G peak (A_D/A_G) is a well established proxy for graphene "quality." As Figure 1(a) illustrates, exposing the Al_2O_3 substrate to a Ni flux of 5×10^{12} atoms/cm^2·s during graphene growth at 950 °C reduces the relative intensity of the D peak by a factor of ~2. The D peak intensity ratio as a function of applied Ni flux for growth at 950 °C is summarized in Figure 1(b), which shows that it steadily decreases with increasing Ni flux, dropping from 2.6 in the absence of Ni to 1.2 when a Ni flux of 7.6×10^{12} atoms/cm^2·s is used. The full-width-at-half-maximum (FWHM, or "Γ") of the Raman peaks, which is a second commonly used indicator of crystalline quality, remain steady regardless of the Ni flux used during growth at 950 °C (Table I). Exposing the substrate to a Ni flux during growth at 850 °C also leads to a decrease in the A_D/A_G ratio (Figure 2). However, the dependency of the A_D/A_G ratio on the Ni flux is much less than at the higher substrate temperature. The Raman

TABLE I. The widths of Raman peaks from graphene films grown under various Ni fluxes.

T_{sub} (°C)	Φ_{Ni} (atoms/cm^2·s)	Γ_D (cm^{-1})	Γ_G (cm^{-1})	Γ_{2D} (cm^{-1})
950	0–7.6×10^{12}	26.5 ± 0.5	19.2 ± 0.2	41.2 ± 0.7
850	0	34.3	37.4	66.5
850	2.5×10^{12}	35.8	40.1	69.9
850	3.7×10^{12}	37.7	44.3	75.6
850	5.5×10^{12}	40.0	46.0	79.3

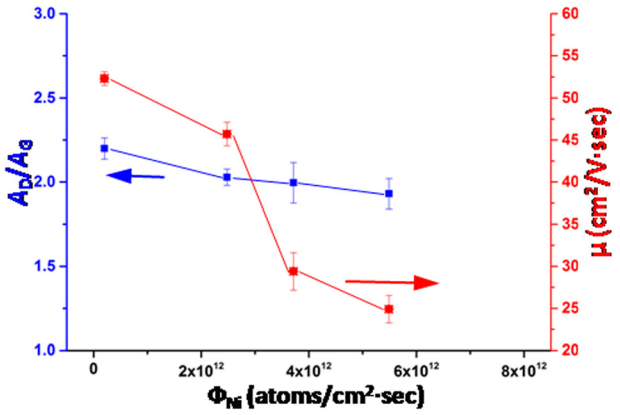

FIG. 2. A summary of the A_D/A_G ratio and charge carrier mobility as a function of applied Ni flux in graphene films grown at 850 °C. Although the A_D/A_G ratio slightly improves with increasing Ni fluxes, the charge carrier mobility steadily decreases ($\lambda = 473$ nm).

peaks from films grown at 850 °C are much wider than those grown at 950 °C, and unlike in the case of the higher substrate temperature they become wider with increasing the Ni flux (Table I).

In addition to the A_D/A_G ratio, the mobility of free charge carriers was used as a second quantitative measure of the crystalline quality of the graphene films. Because the entire 1 cm × 1 cm film is sampled in the van der Pauw geometry, these mobilities are averages; local measurements such as lithographically patterned Hall bars might yield higher values. The films were found to be universally *p*-type, with a steady carrier concentration of $(1.0–1.2) \times 10^{13}\,\mathrm{cm}^{-2}$ regardless of growth conditions. This is consistent with previous reports for graphene on Al_2O_3,[17] indicating that the film-substrate interactions dominate in determining the final carrier concentration. As Figure 1(b) shows, the dependence of the mobility on the Ni flux follows an inverse trend to the A_D/A_G ratio for growth at 950 °C. The mobility steadily improves with increasing Ni flux, going from $49\,\mathrm{cm}^2/\mathrm{V}\cdot\mathrm{s}$ without a Ni flux to a maximum of $79\,\mathrm{cm}^2/\mathrm{V}\cdot\mathrm{s}$ for a Ni flux of 5×10^{12} atom/cm^2·s. Films grown under a Ni flux higher than this at 950 °C were found to be not conductive, which is likely related to morphological changes in the substrate surface at these higher Ni fluxes, as will be discussed later. Rather than leading to an improvement, applying a Ni flux during growth at 850 °C reduced the charge carrier mobility, with higher Ni fluxes producing progressively larger reductions (Figure 2).

X-ray photoelectron spectroscopy confirmed the absence of detectable levels of residual Ni following growth and allowed the examination of the binding states within the graphene film itself. As the survey spectrum in Figure 3(a) shows, no Ni was observed to have persisted on the sample surface in either a metallic state or bound with substrate material in Ni-Al-O compounds. (This specific film was grown at 950 °C under a Ni flux of 5×10^{12} atoms/cm^2·s.) This verifies that minimal Ni remained on the sample surface after flux exposure was halted at the conclusion of C deposition, having either re-evaporated or, possibly, diffused into the Al_2O_3 substrate. Given the characteristics of the specific XPS system used here, we estimate the detection limit for Ni below monolayer graphene to be in the order of 1/40 of a monolayer. The high growth temperature and the absence of bulk-like Ni (i.e., large droplets or islands) preclude the formation of the Ni_2C surface carbide phase, which might compete with graphene formation.[18,19] XPS also shows no evidence of detectable quantities of C intermixing with the substrate leading to Al-C or Al-O-C species, in agreement with previous XPS results on graphene grown by MBE on Al_2O_3(0001).[17]

An examination of the C1s peak in the XPS spectrum shows it to be dominated by the signal of sp^2 configured C and shifted slightly (0.3 eV) to lower binding energies as compared to graphite,[20] consistent with the *p*-type doping level observed in transport. The C1s photoemission signal from this film also displays the lowest intensity defect component—situated at slightly higher binding energies than the peak C1s intensity[21]—yet observed for films grown on dielectric substrates in this MBE. Figure 3(b) also presents the C1s spectrum of the film with the lowest previously observed

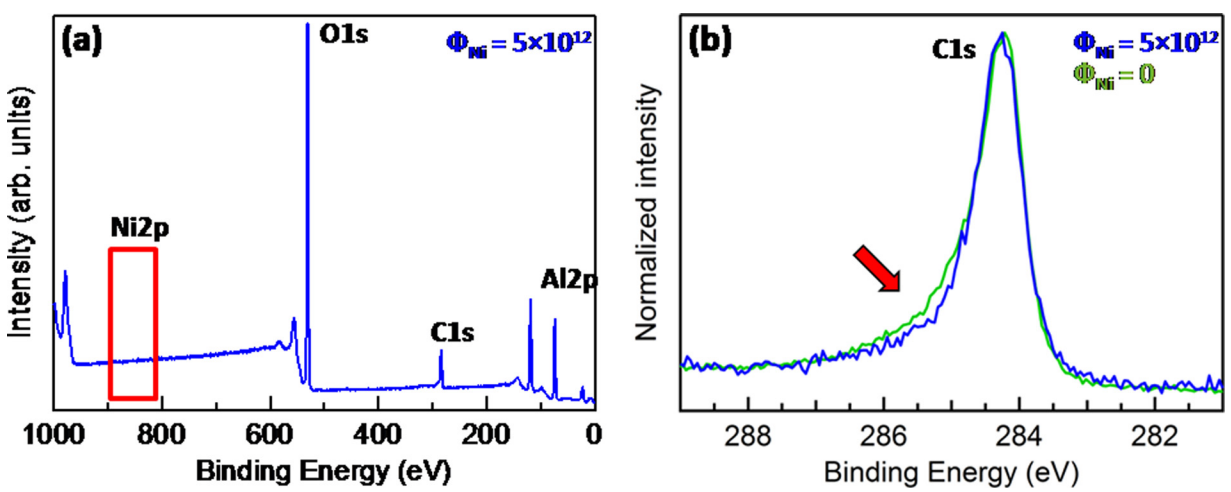

FIG. 3. XPS spectra showing no remaining Ni is detectable at the completion of film growth (a). A close examination of the C1s level displays a lower intensity defect component at higher binding energies (red arrow) than has been previously observed in graphene grown on Al_2O_3(0001) in this MBE (b). The latter is included for comparison.[17]

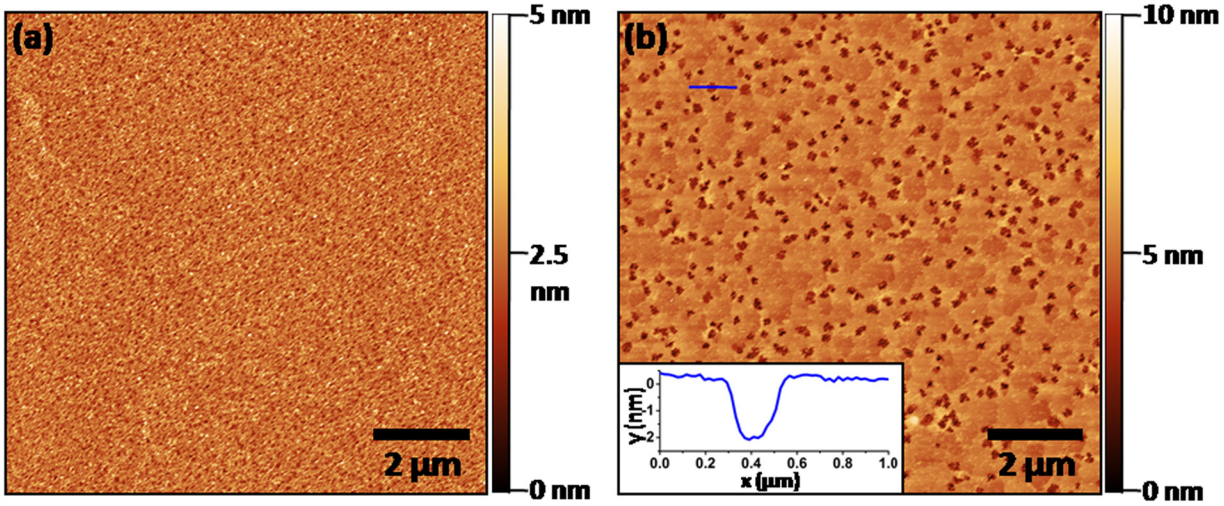

FIG. 4. AFM examining graphene films grown in the absence of Ni (a), and in the presence of a Ni flux (b). Growth without Ni and at low Ni fluxes leads to a slight but homogeneous increase in surface roughness. At higher Ni fluxes "pits" begin to form in the $Al_2O_3(0001)$ substrate surface (see cross section inset in (b), $\Phi_{Ni} = 7.6 \times 10^{12}$ atoms/cm^2·s).

defect component for comparison, which was 3 monolayers thick and grown at a 50 °C higher substrate temperature.[17] Note that the spectra of the samples with and without Ni flux were normalized to the same height and the latter shifted by −0.13 eV to facilitate comparison of the peak shapes. A decreased intensity of the defect component observed via XPS is consistent with the increase in structural order indicated by the lower A_D/A_G ratio in Raman for films grown under a Ni flux. It should be noted that surface contaminants accumulated during atmospheric exposure may also lead to broadening of the C1s peak.[22] Reduced adhesion of atmospheric contaminants caused by the increased structural order of graphene films grown under a Ni flux could also play a role in the C1s trend observed here. As mentioned, the films were annealed at 400 °C in UHV prior to XPS collection to minimize surface contamination, and the consistent doping level suggests this was largely effective.

The morphology of the graphene films was examined by AFM. These scans reveal a slight roughening of the surface compared to bare $Al_2O_3(0001)$ for films grown without Ni and at lower Ni fluxes (Figure 4(a)), with slight localized variations in film thickness possibly contributing. However, a more dramatic surface evolution is observed when higher Ni fluxes are used at a substrate temperature of 950 °C. Rather than a slightly rougher but uniform surface, these samples contain "pits" which are 2–5 nm deep and 100–200 nm across (Figure 4(b)). The onset of pitting occurs at a Ni flux between 5×10^{12} and 7.6×10^{12} atoms/cm^2·s (for growth at 950 °C). Pitting was not observed in samples grown at 850 °C. Consistent with XPS, AFM offers no evidence of significant quantities of residual surface Ni such as Ni islands.

IV. DISCUSSION

The reduction in integrated intensity of the Raman D peak and increased charge carrier mobility in films grown at 950 °C shows that an externally applied Ni flux can enhance the structural quality of graphene grown directly on $Al_2O_3(0001)$ by MBE. To understand in greater detail how this occurs, we first reexamine the Raman data presented here in the context of existing reports regarding spectroscopy of defects in graphene. Specifically, we consider separately the response of the maximum peak intensity ratio (I_D/I_G, as opposed to the integrated area A_D/A_G) and the widths of the Raman peaks (Γ_G, Γ_D, Γ_{2D}) to two distinct types of structural disorder: point defects and reduced grain size. Point defects in the graphene lattice may be parameterized by their average spacing "L_D," while the size of the domains is described by their average lateral size "L_a." Both types of defects contribute to increasing I_D/I_G as well as the width of the Raman peaks. However, while an increasing concentration of point defects leads to a higher I_D/I_G ratio, it does not appreciably widen the Raman peaks until L_D reaches ∼5 nm or less.[23] This threshold coincides approximately with the transition from stage 1 to stage 2 in the amorphization trajectory of sp^2 C first described by Ferrari and Robertson,[24] and further elaborated upon by others.[23,25] In stage 1, the intensity of the D peak is proportional to the total number of defects probed by the laser spot, and the contribution to I_D/I_G from different defects and defect types is additive. This is not the case in stage 2, where the defect density is sufficiently high that an electron-hole pair is likely to be scattered by a second defect prior to encountering a phonon. The delayed onset of peak widening with decreasing L_D is significant because point defects may increase I_D/I_G without simultaneously causing peak broadening, and this is exactly the situation observed here for growth at 950 °C.

In addition to remaining constant regardless of the Ni flux, the narrow Γ_D, Γ_G, and Γ_{2D} values (see Table I) of films grown at 950 °C also indicate that point defects are not present in sufficient quantity to contribute to widening the Raman peaks. This places the films well within stage 1 of the amorphization trajectory. Because of this it is possible to quantitatively evaluate the impact of an externally applied Ni flux on both the domain size (L_a) and point defect concentration (L_D) of the nanocrystalline graphene. First, the semi-

empirical relationship developed by Cançado *et al.*[26] is used to determine the average lateral size of the constituent domains in these films

$$\Gamma\,(\mathrm{cm}^{-1}) = A + \frac{B}{L_a}. \tag{1}$$

With the unique constants (A (cm^{-1}) and B (cm^{-1}·nm) from Ref. 26) inserted for each different Γ we find $L_a = (67 \pm 1.5)$ nm. Because the peak widths do not vary with Ni flux, this is the average domain size in each film grown at 950 °C. The contribution from the finite domain size to the total observed A_D/A_G ratio can then be calculated with the relationship

$$L_a(\mathrm{nm}) = \frac{560}{E_l^4}\left(\frac{A_D}{A_G}\right)^{-1}, \tag{2}$$

where E_l is the energy of the excitation laser (2.62 eV, in this case).[27] As the defect contributions to Raman scattering are additive in stage 1, the contribution to the total D peak intensity (i.e., A_D/A_G) solely from point defects can be isolated; $A_D/A_G = 2.39$ in the absence of Ni, and $A_D/A_G = 1.21$ for an optimal Ni flux of 5×10^{12} atoms/cm^2·s. The average spacing between point defects may then be determined via[23]

$$L_D^2(\mathrm{nm}^2) = \frac{(4.3 \pm 1.3) \times 10^3}{E_l^4}\left(\frac{I_D}{I_G}\right)^{-1}. \tag{3}$$

Note that the equation above is formulated for I_D/I_G, requiring A_D/A_G to be converted using the relation

$$\frac{I_D}{I_G} = \frac{A_D}{A_G} \times \frac{\Gamma_G}{\Gamma_D}. \tag{4}$$

This analysis indicates L_D rose from 7.3 ± 2.0 nm to 10.2 ± 2.8 nm, corresponding to a drop in point defect concentration from $(6.0 \pm 1.7) \times 10^{11}$ to $(3.0 \pm 0.8) \times 10^{11}$ defects/cm^2. Given that other types of defects not considered here likely contribute to the disorder indicated by the Raman spectra, these are conservative estimates for L_D and L_a. The application of an external Ni flux thus reduced the concentration of point defects in the graphene films by ~50%.

The decrease in point defect concentration is corroborated by other related features in the Raman spectra, which also indicate that lattice vacancies are the dominant point defect. Eckmann *et al.* have shown that the maximum intensity of the D′ peak varies in relation to that of the D peak ($I_D/I_{D'}$) according to the specific type of defect present; with reduced domain size leading to a $I_D/I_{D'}$ ratio of ~3.5, lattice vacancies ~7, and sp^3hybridization sites ~13.[25] The initial $I_D/I_{D'}$ ratio of 6.3 seen in films grown here at 950 °C without Ni indicates that vacancies are responsible for the majority of Raman scattering, with a smaller contribution from the reduced grain size. Significantly, the $I_D/I_{D'}$ ratio drops to 4.9 in films grown under a Ni flux of 5×10^{12} atoms/cm^2·s, showing that an increasing proportion of defect scattering results from the ~67 nm grain size as opposed to lattice vacancies. The reduced $I_D/I_{D'}$ ratio further verifies the interpretation that an externally applied Ni flux reduces the vacancy concentration in graphene films grown at 950 °C.

The benefit derived from the Ni saturated at a given flux, with additional Ni leading to non-conducting films. This transition coincided with the onset of substrate pitting during growth. The reaction products from the substrate pitting (including O) may have reacted with the C, leading to partial C desorption. The increased surface roughness could also geometrically prevent a continuous film from forming. Thus, the chemical stability of the dielectric substrate may be a limiting factor in determining the maximum beneficial Ni flux. This interpretation is consistent with the results of graphene growths also performed under a Ni flux on two less chemically stable dielectric substrates, MgO(111) and SiO_2 (not shown), both of which resulted in substantially decreased graphene quality. Experiments examining whether other dielectrics, such as h-BN, allow higher Ni fluxes to be effective are ongoing.

The peaks in the Raman spectra of films grown at 850 °C are much wider than those grown at 950 °C, sufficiently so to place the films in stage 2 of the amorphization trajectory. Because the Tuinstra and Koenig relation is not applicable in stage 2, the A_D/A_G ratio is no longer a reliable indicator of crystalline quality.[24,28] This explains how the A_D/A_G ratio and μ do not show the same trend with respect to Φ_{Ni} in Figure 2 as they do in Figure 1(b). The contributions of different defect types also no longer sum independently in stage 2, preventing any quantitative estimation of the influence of the Ni flux. However, the combination of increasing Raman peak widths and decreasing mobility with Φ_{Ni} is qualitatively consistent with an overall reduction in film quality at the lower growth temperature. We speculate that the limited surface diffusion—and associated reduction in grain size—from the lower substrate temperature lead to such a disordered growth surface that Ni is ineffective at limiting vacancy formation.

It has proven challenging to identify the precise atomistic mechanism through which the Ni flux reduces the lattice point defect concentration. Depositing a graphene film and subsequently annealing it under a Ni flux did not produce a similar decrease in structural disorder. Likewise, the modest graphene domain size ((67 ± 1.5) nm) and the fact that it does not vary with applied Ni flux—even in the case when no Ni was used—suggests that while Ni may play some role in the graphene nucleation process, this is not its dominant impact. The interactions between Ni and C which lead to increased crystalline quality must thus occur during the process of their incorporation into the graphene lattice. Ideally, XPS would reveal the details of the chemical interactions between Ni, C, and Al_2O_3(0001) substrate during growth, but *in situ* capabilities were not available and the absence of detectable Ni means post-growth analysis is not effective in this respect. Efforts to monitor the growth surface during deposition using other methods, such as reflection high-energy electron diffraction, were equally unilluminative. However, useful insights may still be extracted by combining a phenomenological view of the growth process used here with existing reports in the literature.

While the limited surface diffusion during graphene growth on dielectrics dominates the resulting microstructure, this is not the case in all growth environments. Metallic

substrates such as Ir(111) and Cu(001) can offer insights into the fundamental mechanisms of graphene formation when they are not masked by the consequences of limited adatom mobility.[29,30] Graphene growth on metals is often "attachment limited," where the incorporation of C adatoms into the graphene lattice at the growth front is the rate-limiting step in the expansion of the crystal. The imperfect execution of this complex process, which can require the formation and simultaneous incorporation of multi-atom clusters, is what introduces vacancies into the lattice. Although little is known about adatom attachment during growth on Al_2O_3, Ni acting catalytically to lower the kinetic barrier of a similarly complex process would be consistent with the reduction in lattice vacancies observed here.

The authors are aware of no previous examinations which have attempted to isolate the surfactant properties of surface metals during graphene growth from their other potential impacts, such as decomposing chemical precursors during CVD growth, but reports do exist which have commonality with the growth conditions used here. Simulations have shown that the presence of Ni atoms lowers the activation barrier for defect healing or formation in the graphene lattice.[31,32] The kinetic similarities between defect healing and adatom incorporation lend credence to the interpretation that the Ni flux used here reduces lattice vacancies. Teng *et al.* investigated the growth of graphene on insulators by CVD when Cu foil is placed in the tube furnace up-stream from the substrate,[33] and Yen *et al.* performed a similar study with a Ni ingot replacing the Cu foil.[34] Teng *et al.* focused primarily on examining the influence of various parameters (such as the distance between the substrate and the Cu foil) on the resulting growth, including the accumulation of Cu on the graphene/substrate surface during particularly long growth runs. However, isolating the impact of the surface Cu is complicated by the mixed environment present during growth, including partially decomposed hydrocarbon precursors and hydrogen gas, which is known to etch carbon.[35] Regardless of this additional complexity and as the author's note, it is likely the presence of Cu on the growth surface resulted in interactions with the growing graphene, possibly contributing to improved crystalline quality. Other methods to take advantage of metal enhancement during graphene growth directly on dielectrics have typically used continuous metal films in various geometries which are chemically removed or evaporated after growth, giving them little bearing on the work presented here.[36,37]

V. CONCLUSION

This study examined whether Ni is an effective surfactant during graphene growth by MBE. We have established that depositing a graphene film under a Ni flux leads to less disorder in the nanocrystalline microstructure, as judged by both Raman spectroscopy and charge carrier mobility. Raman also indicates that the reduction in structural disorder is due to fewer lattice vacancies, while the domain size stays constant. This is consistent with the surface Ni atoms acting to assist adatom incorporation into the graphene lattice. The use of metal surfactants, such as Ni, offers an alternate pathway to make the improvements in the quality of graphene films grown directly on dielectric substrates necessary for their use in technological applications.

ACKNOWLEDGMENTS

The authors would like to thank Dr. Esperanza Luna for her critical reading of the manuscript, and H.-P. Schönherr, M. Höricke, and C. Herrmann for technical support. J.M.W. acknowledges support from the Leibniz Association and Alexander von Humboldt Foundation.

[1]A. C. Ferrari, F. Bonaccorso, V. Falko, K. S. Novoselov, S. Roche, P. Bøggild, S. Borini, F. Koppens, V. Palermo, N. Pugno, J. A. Garrido, R. Sordan, A. Bianco, L. Ballerini, M. Prato, E. Lidorikis, J. Kivioja, C. Marinelli, T. Ryhänen, A. Morpurgo, J. N. Coleman, V. Nicolosi, L. Colombo, A. Fert, M. Garcia-Hernandez, A. Bachtold, G. F. Schneider, F. Guinea, C. Dekker, M. Barbone, C. Galiotis, A. Grigorenko, G. Konstantatos, A. Kis, M. Katsnelson, C. W. J. Beenakker, L. Vandersypen, A. Loiseau, V. Morandi, D. Neumaier, E. Treossi, V. Pellegrini, M. Polini, A. Tredicucci, G. M. Williams, B. H. Hong, J. H. Ahn, J. M. Kim, H. Zirath, B. J. van Wees, H. van der Zant, L. Occhipinti, A. Di Matteo, I. A. Kinloch, T. Seyller, E. Quesnel, X. Feng, K. Teo, N. Rupesinghe, P. Hakonen, S. R. T. Neil, Q. Tannock, T. Löfwander, and J. Kinaret, Nanoscale **7**, 4598 (2015).
[2]K. Saito and T. Ogino, J. Phys. Chem. C **118**, 5523 (2014).
[3]E. Moreau, S. Godey, F. J. Ferrer, D. Vignaud, X. Wallart, J. Avila, M. C. Asensio, F. Bournel, and J.-J. Gallet, Appl. Phys. Lett. **97**, 241907 (2010).
[4]G. Lippert, J. Dabrowski, Y. Yamamoto, F. Herziger, J. Maultzsch, M. C. Lemme, W. Mehr, and G. Lupina, Carbon **52**, 40 (2013).
[5]J.-H. Lee, E. K. Lee, W.-J. Joo, Y. Jang, B.-S. Kim, J. Y. Lim, S.-H. Choi, S. J. Ahn, J. R. Ahn, M.-H. Park, C.-W. Yang, B. L. Choi, S.-W. Hwang, and D. Whang, Science **344**, 286 (2014).
[6]F. Maeda and H. Hibino, Jpn. J. Appl. Phys. **49**, 04DH13 (2010).
[7]S.-K. Jerng, D. Seong Yu, J. Hong Lee, C. Kim, S. Yoon, and S.-H. Chun, Nanoscale Res. Lett. **6**, 565 (2011).
[8]E. Moreau, F. J. Ferrer, D. Vignaud, S. Godey, and X. Wallart, Phys. Status Solidi **207**, 300 (2010).
[9]M. Zhou, F. L. Pasquale, P. A. Dowben, A. Boosalis, M. Schubert, V. Darakchieva, R. Yakimova, L. Kong, and J. A. Kelber, J. Phys.: Condens. Matter **24**, 072201 (2012).
[10]M. Copel, M. Reuter, E. Kaxiras, and M. Tromp, Phys. Rev. Lett. **63**, 632 (1989).
[11]P. G. Evans, O. D. Dubon, J. F. Chervinsky, F. Spaepen, and J. A. Golovchenko, Appl. Phys. Lett. **73**, 3120 (1998).
[12]R. J. Koch, M. Weser, W. Zhao, F. Viñes, K. Gotterbarm, S. M. Kozlov, O. Höfert, M. Ostler, C. Papp, J. Gebhardt, H.-P. Steinrück, A. Görling, and T. Seyller, Phys. Rev. B **86**, 075401 (2012).
[13]J. J. Lander, H. E. Kern, and A. L. Beach, J. Appl. Phys. **23**, 1305 (1952).
[14]J. Wintterlin and M.-L. Bocquet, Surf. Sci. **603**, 1841 (2009).
[15]R. E. Honig and D. A. Kramer, RCA Rev. **30**, 285 (1969).
[16]A. C. Ferrari, J. C. Meyer, V. Scardaci, C. Casiraghi, M. Lazzeri, F. Mauri, S. Piscanec, D. Jiang, K. S. Novoselov, S. Roth, and A. K. Geim, Phys. Rev. Lett. **97**, 187401 (2006).
[17]M. H. Oliveira, T. Schumann, R. Gargallo-Caballero, F. Fromm, T. Seyller, M. Ramsteiner, A. Trampert, L. Geelhaar, J. M. J. Lopes, and H. Riechert, Carbon **56**, 339 (2013).
[18]P. Jacobson, B. Stöger, A. Garhofer, G. S. Parkinson, M. Schmid, R. Caudillo, F. Mittendorfer, J. Redinger, and U. Diebold, ACS Nano **6**, 3564 (2012).
[19]L. L. Patera, C. Africh, R. S. Weatherup, R. Blume, S. Bhardwaj, C. Castellarin-Cudia, A. Knop-Gericke, R. Schloegl, G. Comelli, S. Hofmann, and C. Cepek, ACS Nano **7**, 7901 (2013).
[20]G. K. Wertheim, P. M. T. M. Van Attekum, and S. Basu, Solid State Commun. **33**, 1127 (1980).
[21]H. Estrade-Szwarckopf, Carbon **42**, 1713 (2004).
[22]R. Blume, D. Rosenthal, J.-P. Tessonnier, H. Li, A. Knop-Gericke, and R. Schloegl, ChemCatChem **7**, 2871 (2015).
[23]L. G. Cançado, A. Jorio, E. H. M. Ferreira, F. Stavale, C. Achete, R. B. Capaz, M. V. O. Moutinho, A. Lombardo, T. S. Kulmala, and A. C. Ferrari, Nano Lett. **11**, 3190 (2011).
[24]A. Ferrari and J. Robertson, Phys. Rev. B **61**, 14095 (2000).

[25]A. Eckmann, A. Felten, A. Mishchenko, L. Britnell, R. Krupke, K. S. Novoselov, and C. Casiraghi, Nano Lett. **12**, 3925 (2012).
[26]L. Cançado, A. Jorio, and M. Pimenta, Phys. Rev. B **76**, 064304 (2007).
[27]L. G. Canc¸ado, K. Takai, T. Enoki, M. Endo, Y. A. Kim, H. Mizusaki, A. Jorio, L. N. Coelho, R. Magalhães-Paniago, and M. A. Pimenta, Appl. Phys. Lett. **88**, 163106 (2006).
[28]F. Tuinstra, J. Chem. Phys. **53**, 1126 (1970).
[29]E. Loginova, N. C. Bartelt, P. J. Feibelman, and K. F. McCarty, New J. Phys. **11**, 063046 (2009).
[30]J. M. Wofford, S. Nie, K. F. McCarty, N. C. Bartelt, and O. D. Dubon, Nano Lett. **10**, 4890 (2010).
[31]D. W. Boukhvalov and M. I. Katsnelson, Appl. Phys. Lett. **95**, 023109 (2009).
[32]S. Karoui, H. Amara, C. Bichara, and F. Ducastelle, ACS Nano **4**, 6114 (2010).
[33]P.-Y. Teng, C.-C. Lu, A.-H. Kotone, Y.-C. Lin, C.-H. Yeh, K. Suenaga, and P. Chiu, Nano Lett. **12**, 1379 (2012).
[34]W.-C. Yen, Y.-Z. Chen, C.-H. Yeh, J.-H. He, P.-W. Chiu, and Y.-L. Chueh, Sci. Rep. **4**, 4739 (2014).
[35]I. Vlassiouk, M. Regmi, P. Fulvio, S. Dai, P. Datskos, G. Eres, and S. Smirnov, ACS Nano **5**, 6069 (2011).
[36]A. Ismach, C. Druzgalski, S. Penwell, A. Schwartzberg, M. Zheng, A. Javey, J. Bokor, and Y. Zhang, Nano Lett. **10**, 1542 (2010).
[37]J. Hofrichter, B. N. Szafranek, M. Otto, T. J. Echtermeyer, M. Baus, A. Majerus, V. Geringer, M. Ramsteiner, and H. Kurz, Nano Lett. **10**, 36 (2010).